RSC Mechanochemistry

ROYAL SOCIETY OF CHEMISTRY

COMMUNICATION

View Article Online
View Journal

Cite this: DOI: 10.1039/d5mr00114e

Received 9th September 2025
Accepted 20th March 2026

DOI: 10.1039/d5mr00114e

rsc.li/RSCMechanochem

Ball milling enables phase-pure synthesis of a temperature sensitive ternary chloride, $MgZrCl_6$

Christopher L. Rom, †*[a] Austin M. Shotwell, †[b] Sinclair R. Combs, [b] Autumn Peters, [c] Lauren Borgia, [c] Hannah M. Martin, [b] Michael P. Moghadasnia, [b] James R. Neilson [cd] and Annalise E. Maughan *[ab]

Ball milling is a powerful synthetic tool for discovering new inorganic materials. Inspired by the high ionic conductivity in Li_2ZrCl_6 synthesized *via* mechanochemistry, we synthesized $MgZrCl_6$ with a similar method. High resolution synchrotron X-ray diffraction shows that $MgZrCl_6$ is poorly crystalline after ball milling, but crystallizes in a layered hexagonal structure ($P\bar{3}1c$) after heat treatment. *In situ* synchrotron X-ray diffraction and differential scanning calorimetry measurements reveal a narrow temperature window around 400 °C in which crystallization occurs. Pair distribution function analysis shows 2D sheets of $MgZrCl_6$ form after milling, with heating driving 3D crystallization. Raman spectroscopy also shows evidence of Zr–Cl octahedral coordination familiar to $MgZrCl_6$ after milling. Electrochemical impedance spectroscopy does not reveal ionic conductivity in $MgZrCl_6$ (limit of detection *ca.* 1.4×10^{-8} S cm^{-1}). In addition to supporting existing design rules for Mg-based solid electrolytes, this work shows the power of ball milling to synthesize temperature-sensitive inorganic compounds with high yield.

Introduction

While traditional solid-state synthesis techniques rely on high temperatures to drive solid-state diffusion, ball milling can drive inter-diffusion between solids at low temperatures. Therefore, the mechanochemical technique can be an atomically efficient process for synthesizing materials ranging from halide perovskites for optoelectronic applications[9,10] to solid electrolytes for batteries. Leading Li- and Na-based solid electrolytes, such as sulfide argyrodites,[11] ternary chlorides,[12] and oxychlorides,[13] have been synthesized *via* ball milling. However, solid-state Mg electrolytes remain a nascent research topic[14] which ball milling may expand.

Chlorides have emerged as a promising class of materials for Li^+ solid electrolytes owing to their high ionic conductivity, low electronic conductivity, and high oxidative stability,[15] but are underexplored for Mg^{2+} conductivity. To the best of our knowledge, MgM_2Cl_8 phases (M = Al, Ga) are the only chlorides that have been studied as Mg^{2+} ion conductors.[16,17] They were synthesized *via* high-temperature solid-state techniques and exhibit ionic conductivity *ca.* 10^{-6} to 10^{-5} S cm^{-1} at 127 °C. Although these few examples underperform leading selenide[18] and borohydride[19] materials, further exploration of chlorides is warranted. Solid state synthesis methods yielded chlorides with low-to-moderate Li^+ ion conductors in the 1990's, but the ball milling synthesis of Li_3YCl_6 produced a fast ion conductor in 2018 and started a renaissance of chloride-based solid electrolytes.[15,20]

$MgZrCl_6$ has a layered structure that may be conducive to Mg^{2+} mobility (Fig. 1), but it has not been studied for this property. We first noticed this phase as an intermediate in the metathesis reaction: $2Mg_2NCl + ZrCl_4 \rightarrow MgZrN_2 + 3MgCl_2$.[21] A 2014 report by Salyulev and Vovkotrub noted that $MgZrCl_6$ was previously studied to better understand corrosion in chloride-based metallurgical processes,[22] and they referenced synthesis literature for these phases from the 1990's.[23,24] We have not been

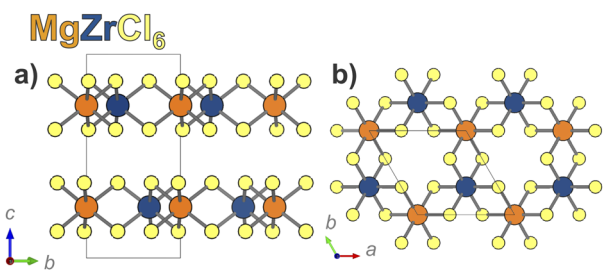

Fig. 1 (a) View of the $MgZrCl_6$ structure down the *a* axis. (b) View of one layer of the structure looking down the *c* axis.

[a]*Materials Science Center, National Laboratory of the Rockies, Golden, CO, 80401, USA. E-mail: christopher.rom@nrel.gov*

[b]*Department of Chemistry, Colorado School of Mines, Golden, CO, 80401, USA. E-mail: amaughan@mines.edu*

[c]*Department of Chemistry, Colorado State University, Fort Collins, CO, 80523, USA*

[d]*School of Materials Science & Engineering, Colorado State University, Fort Collins, CO, 80523, USA*

† C. L. R. and A. M. S. contributed equally.

able to access these original synthesis reports, but the 2014 report suggests that $MgZrCl_6$ was synthesized using elevated $ZrCl_4$ vapor pressures (*ca.* 22–59 atm) and in narrow temperature ranges (*ca.* 450–500 °C).[22] Given the volatility of $ZrCl_4$ (sublimation point, 331 °C), we hypothesized that mechanochemistry may provide a route to phase pure $MgZrCl_6$.

Results and discussion

High-resolution synchrotron powder X-ray diffraction (PXRD) shows that 10 h of high-energy ball milling (BM) of $MgCl_2$ + $ZrCl_4$ produced poorly crystalline $MgZrCl_6$ (Fig. 2). ZrO_2 jars and balls were used for milling (more details in SI). Subsequent heat treatment (BM + HT) crystallizes $MgZrCl_6$ in space group $P\bar{3}1c$ (a = 6.35975(3) Å and c = 11.8428(1) Å), isostructural with $FeZrCl_6$ (inorganic crystal structure database col. code 39666).[3] Ball milling was crucial for the synthesis of phase pure $MgZrCl_6$, as hand-ground mixtures of reagents only reacted partially (Fig. S1 and S2).

The crystal structure of $MgZrCl_6$ (BM + HT) consists of layers stacked along the c direction, with each layer containing edge-sharing [$MgCl_6$] and [$ZrCl_6$] octahedra. Within the layer, 2/3 of the octahedral sites are occupied with an alternating pattern of Mg^{2+} and Zr^{4+}, while the remaining 1/3 of octahedral sites are vacant. Consequently, each Mg^{2+} is neighbored by three Zr^{4+} and three vacant octahedra. The chloride anions form a hexagonal close-packed arrangement with a van der Waals gap between the layers. We note three significant peaks in the difference trace, indicating that the (002), (2$\bar{1}$2), and (300) Bragg peaks are under-fit by our model. Our attempts to improve our model with stacking faults, anisotropic peak broadening, and cation-disorder, were unsuccessful. We also considered a structural model based on $TlYbI_6$ (ICSD col. code 138835), which also crystallizes in the $P\bar{3}1c$ space group but with different atomic coordinates: that model was substantially worse. It is possible for cations to disorder into van der Waals gap,[25] but our attempts to refine electron density in inter-layer sites did not substantially improve the fit. Single crystal diffraction measurements may be needed to more precisely determine the structure.

In situ synchrotron PXRD shows the crystallization and decomposition pathway for $MgZrCl_6$ from ball milled precursors (Fig. 3). Broad peaks are present at room temperature, indicating that ball milling resulted in a poorly crystalline ternary phase. At 340 °C, the broad peaks of the initial phase sharpen, and additional reflections appear as $MgZrCl_6$ rapidly crystallizes. At 460 °C, the $MgZrCl_6$ peaks abruptly disappear, leaving behind only $MgCl_2$. This change shows that $MgZrCl_6$ has limited thermal stability, decomposing to $MgCl_2$ (s) and $ZrCl_4$ (g) at moderate temperatures. These *in situ* findings are consistent with our *ex situ* results (Fig. S1) and with differential scanning calorimetry (DSC) measurements (Fig. S9).

Pair distribution function (PDF) analysis of X-ray total scattering data suggest that BM $MgZrCl_6$ has a similar local structure to BM + HT $MgZrCl_6$ (Fig. 4). The BM + HT sample exhibits short and long range pair correlations that are well fit by the $P\bar{3}1c$ $MgZrCl_6$ model (Fig. 4a). The PDF of the ball milled sample reveals significantly attenuated pair correlations beyond $r \approx 6$ Å. Furthermore, the bulk crystal structure does not fit these data well beyond $r \approx 4$ Å, particularly at distances corresponding to the interlayer separations (Fig. S3). Instead, a composite model with a single layer of $MgZrCl_6$ as implemented in PDFGUI[26] following ref. 27 with a spherical truncation diameter of 50(30)

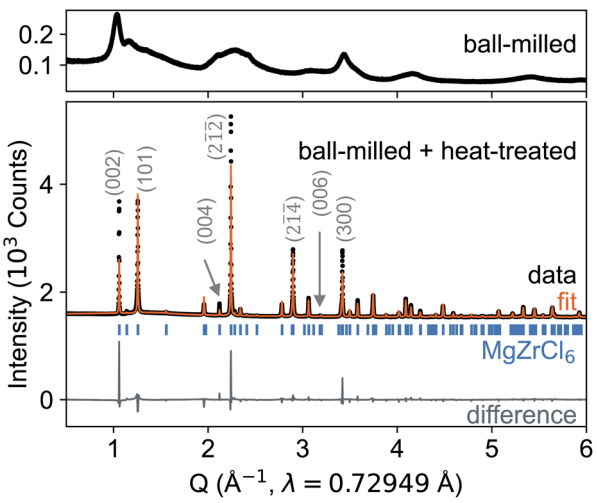

Fig. 2 Synchrotron PXRD of $MgZrCl_6$ prepared by ball milling and the sample after heat treatment at 350 °C for 2 h in a sealed ampule.

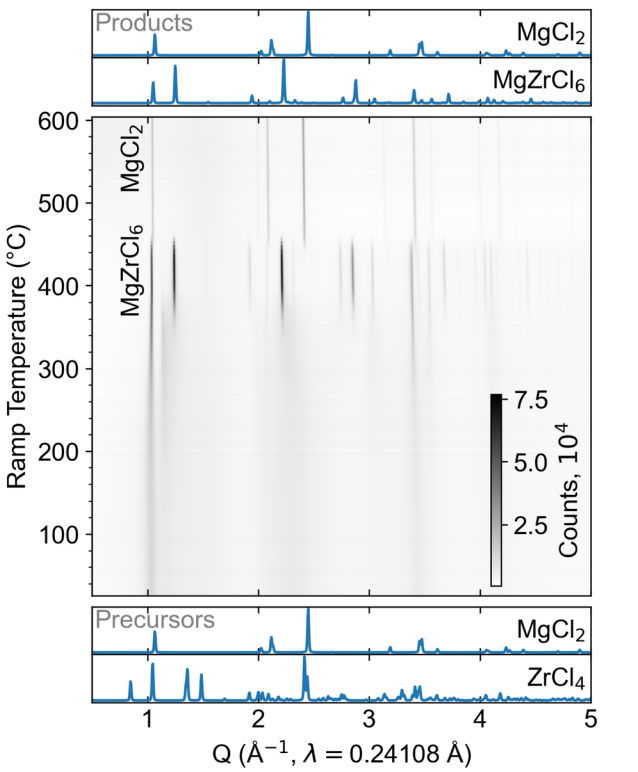

Fig. 3 *In situ* synchrotron PXRD of a BM mixture of $MgCl_2$ + $ZrCl_4$ upon heating at +10 °C min^{-1}. Simulated reference patterns for the precursors and products are shown at the bottom and top, respectively.

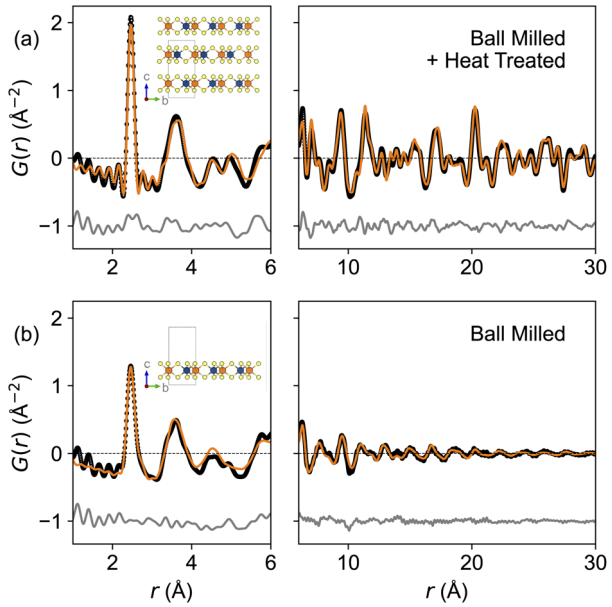

Fig. 4 PDF of X-ray total scattering data from (a) BM + HT samples and (b) BM of $MgZrCl_6$. Data in black, fit in orange, difference in gray (offset vertically by 1 $Å^{-2}$). Insets show structural models.

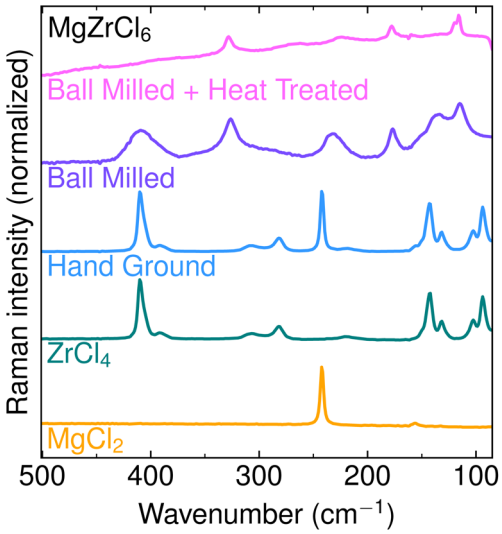

Fig. 5 Background-subtracted Raman spectra of the crystallized $MgZrCl_6$ (BM + HT) and poorly-crystalline ball milled $MgZrCl_6$ compared with the hand-ground precursor mix $MgCl_2$ + $ZrCl_4$ and the binary precursors. Raw spectra are shown in Fig. S4.

Å, provides the best fit to the data (Fig. 4b). A similar result was observed *via* PDF for the initial stages of FeS nanosheet growth from solution.[28] This suggests that ball milling induces formation of $MgZrCl_6$ sheets with octahedral coordination and some Mg–Zr ordering, but annealing is necessary to induce extended ordering. Although poorly-crystalline milled materials "age" in some cases,[29] we do not observe this behavior in $MgZrCl_6$. Laboratory PXRD data of the same ball-milled material collected ~3 years after the synchrotron powder X-ray diffraction data (Fig. 2) exhibits similar broadened features (Fig. S10).

Raman spectroscopy shows that the BM $MgZrCl_6$ has structural motifs that are conserved upon crystallization (Fig. 5). The Raman spectrum of BM + HT $MgZrCl_6$ has peaks at 327 cm^{-1}, 177 cm^{-1}, and 116 cm^{-1}. Similar peaks also appear in the spectrum for the BM $MgZrCl_6$. While we do not precisely assign these vibrational modes, these shared peaks suggest that structural motifs of the crystallized $MgZrCl_6$ are already present in the poorly crystalline material produced by the ball milling step, consistent with PDF analysis. The BM $MgZrCl_6$ spectrum also has broad peaks at 410 cm^{-1}, 232 cm^{-1}, and 135 cm^{-1} that roughly correspond to peaks from the binary halide precursors, suggesting that mechanochemical conversion to $MgZrCl_6$ is incomplete (10 h milling time). In contrast, the spectrum from the hand-ground sample of $MgCl_2$ + $ZrCl_4$ is merely a linear combination of the precursor spectra. These data show that ball milling initiates formation of the $MgZrCl_6$ phase, which crystallizes on heating.

Given the open framework of $MgZrCl_6$ with an ordered arrangement of vacant octahedra within layers and a van der Waals gap between layers (Fig. 1), we hypothesized that Mg^{2+} may be mobile in the structure. We performed AC electrochemical impedance spectroscopy (EIS) in a two-electrode configuration up to 95 °C. The BM and BM + HT $MgZrCl_6$ did not exhibit charge transport behavior (Fig. S6 and S7). Rather, the materials show capacitive behavior consistent with a dielectric. Given the limit of detection for the measurement (approximately 4 MΩ) along with the pellet dimensions (0.71 mm thick, 1.27 cm^2 cross-sectional area), we can rule out ionic conductivity above approximately 1.4 × 10^{-8} S cm^{-1}. We attempted aliovalent substitution of Nb^{5+} into $MgZrCl_6$ in hopes of boosting ionic conductivity (Fig. S7), but the more volatile $NbCl_5$ separated from the pellet during annealing and was not incorporated into the structure.

The negligible ionic conductivity of this phase is consistent with design rules for multivalent ion conductors described in prior literature. Rong *et al.* proposed that Mg^{2+} mobility may be favorable in structures where Mg^{2+} ions sit in energetically-disfavored sites (*i.e.*, tetrahedra).[7] In $MgZrCl_6$, Mg^{2+} occupies an octahedral site, which is more stable and thus less prone to hopping. Iton and See also noted that repulsive forces increase when a mobile ion moves through a site that is face-sharing with a site occupied by a highly-charged cation.[8] The Zr^{4+} sites in $MgZrCl_6$ are face-sharing with 2/3 of the octahedral holes within the van der Waals gap, inhibiting Mg^{2+} mobility within that layer. Bond valence site energy calculations suggest the lowest migration barrier in $MgZrCl_6$ is 0.86 eV for interlayer hopping (Fig. S8). This value is higher than the 0.6 eV cutoff used for prior theoretical work screening for Mg^{2+} ion conductors.[6] Our findings therefore further validate the design rules posed in these prior works.

Although $MgZrCl_6$ proved not to be an Mg^{2+} ion conductor, the synthetic approach may be useful for yielding phase-pure solids that include volatile precursors. Our preliminary work in this Mg–Zr–Cl system motivates further study into other compositions that may be stabilized through mechanochemical methods. In this case, $ZrCl_4$ sublimes at 330 °C, but ball milling can trap it within the $MgZrCl_6$ framework, allowing for

subsequent heat treatment at 350 °C to crystallize the ternary without vapor loss. Many other chlorides also have low boiling or sublimation points, such as $TiCl_4$ (boils at 136 °C), $AlCl_3$ (sublimes at 180 °C), and $NbCl_5$ (boils at 247 °C). Similarly, many bromides and iodides boil, sublime, or decompose at relatively low temperatures. The ball milling approach here may enable the synthesis of other temperature-sensitive halides.

Author contributions

C. L. R. – conceptualization, formal analysis, investigation, visualization, writing – original draft. A. M. S. – formal analysis, investigation, visualization S. R. C. – formal analysis. A. P. – investigation. L. B. – investigation. H. M. M. – investigation. M. P. M. – investigation. J. R. N. – formal analysis. A. E. M. – formal analysis, funding acquisition. All authors edited the manuscript.

Conflicts of interest

There are no conflicts to declare.

Data availability

Data for this article, including diffraction patterns, PDF data, and Raman spectra, are available at FigShare at https://doi.org/10.6084/m9.figshare.c.8023465. Additional data supporting this article have been included as part of the supplementary information (SI). Supplementary information: experimental methods, PXRD analysis, Raman spectroscopy results, bond valence site analysis, differential scanning calorimetry data, and additional ref. 1–8. See DOI: https://doi.org/10.1039/d5mr00114e.

CCDC 2421152 ($MgZrCl_6$) contains the supplementary crystallographic data for this paper.[30]

Acknowledgements

This work was authored by the National Laboratory of the Rockies for the U.S. Department of Energy (DOE), operated under Contract No. DE-AC36-08GO28308. C. L. R. and A. E. M. acknowledge support from the Laboratory Directed Research and Development (LDRD) program at NLR. Thanks to Sita Dugu for helpful discussions of Raman spectroscopy. Use of the Advanced Photon Source at Argonne National Laboratory was supported by the U.S. Department of Energy, Office of Science, Office of Basic Energy Sciences, under Contract no. DE-AC02-06CH11357. Use of the Stanford Synchrotron Radiation Lightsource, SLAC National Accelerator Laboratory, is supported by the U.S. Department of Energy, Office of Science, Office of Basic Energy Sciences under Contract no. DE-AC02-76SF00515. The views expressed in the article do not necessarily represent the views of the DOE or the U.S. Government.

Notes and references

1 C. L. Rom, P. Yox, A. M. Cardoza, R. W. Smaha, M. Q. Phan, T. R. Martin and A. E. Maughan, *Chem. Mater.*, 2024, **36**, 7283–7291.
2 K. H. Stone, M. R. Cosby, N. A. Strange, V. Thampy, R. C. Walroth and C. Troxel Jr, *J. Appl. Crystallogr.*, 2023, **56**, 1480–1484.
3 S. Troyanov, B. Kharisov and S. Berdonosov, *Zh. Neorg. Khim.*, 1992, **37**, 2424–2429.
4 P. J. Chupas, K. W. Chapman, C. Kurtz, J. C. Hanson, P. L. Lee and C. P. Grey, *J. Appl. Crystallogr.*, 2008, **41**, 822–824.
5 P. Juhás, T. Davis, C. L. Farrow and S. J. Billinge, *Appl. Crystallogr.*, 2013, **46**, 560–566.
6 T. Chen, G. Sai Gautam and P. Canepa, *Chem. Mater.*, 2019, **31**, 8087–8099.
7 Z. Rong, R. Malik, P. Canepa, G. Sai Gautam, M. Liu, A. Jain, K. Persson and G. Ceder, *Chem. Mater.*, 2015, **27**, 6016–6021.
8 Z. W. Iton and K. A. See, *Chem. Mater.*, 2022, **34**, 881–898.
9 F. Palazon, Y. El Ajjouri and H. J. Bolink, *Adv. Energy Mater.*, 2020, **10**, 1902499.
10 D. Ceriotti, P. Marziani, F. M. Scesa, A. Collorà, C. L. Bianchi, L. Magagnin and M. Sansotera, *RSC Mechanochem.*, 2024, **1**, 520–530.
11 S. Boulineau, M. Courty, J.-M. Tarascon and V. Viallet, *Solid State Ionics*, 2012, **221**, 1–5.
12 H. Kwak, D. Han, J. Lyoo, J. Park, S. H. Jung, Y. Han, G. Kwon, H. Kim, S.-T. Hong, K.-W. Nam, *et al.*, *Adv. Energy Mater.*, 2021, **11**, 2003190.
13 T. Zhao, B. Samanta, X. M. de Irujo-Labalde, G. Whang, N. Yadav, M. A. Kraft, P. Adelhelm, M. R. Hansen and W. G. Zeier, *ACS Mater. Lett.*, 2024, **6**, 3683–3689.
14 P. W. Jaschin, Y. Gao, Y. Li and S.-H. Bo, *J. Mater. Chem. A*, 2020, **8**, 2875–2897.
15 S. R. Combs, P. K. Todd, P. Gorai and A. E. Maughan, *J. Electrochem. Soc.*, 2022, **169**, 040551.
16 Y. Tomita, R. Saito, A. Nagata, Y. Yamane and Y. Kohno, *Energies*, 2020, **13**, 6687.
17 Y. Tomita, R. Saito, M. Morishita, Y. Yamane and Y. Kohno, *Solid State Ionics*, 2021, **361**, 115566.
18 P. Canepa, S.-H. Bo, G. Sai Gautam, B. Key, W. D. Richards, T. Shi, Y. Tian, Y. Wang, J. Li and G. Ceder, *Nat. Commun.*, 2017, **8**, 1759.
19 E. Roedern, R.-S. Kühnel, A. Remhof and C. Battaglia, *Sci. Rep.*, 2017, **7**, 46189.
20 T. Asano, A. Sakai, S. Ouchi, M. Sakaida, A. Miyazaki and S. Hasegawa, *Adv. Mater.*, 2018, **30**, 1803075.
21 C. L. Rom, M. J. Fallon, A. Wustrow, A. L. Prieto and J. R. Neilson, *Chem. Mater.*, 2021, **33**, 5345–5354.
22 A. B. Salyulev, E. Vovkotrub and E. G. Bobkotrub, *Melts*, 2014, 71–77.
23 A. Salyulev, E. Vovkotrub and V. Strekalovsky, *International Conference on Raman Spectroscopy*, 1998, pp. 714–715.
24 A. B. Salyulev, E. G. Bobkotrub and V. N. Strekalovsky, *J. Inorg. Chem.*, 1990, **35**, 902.
25 H. C. Mandujano, T. Li, P. Y. Zavalij and E. E. Rodriguez, *Chem. Mater.*, 2024, **36**, 5172–5183.
26 C. L. Farrow, P. Juhas, J. W. Liu, D. Bryndin, E. S. Bozin, J. Bloch, T. Proffen and S. J. L. Billinge, *J. Phys.: Condens. Matter*, 2007, **19**, 335219.

27 Z. Chen, M. L. Beauvais and K. W. Chapman, *J. Appl. Crystallogr.*, 2023, **56**, 328–337.
28 M. L. Beauvais, P. J. Chupas, D. O'Nolan, J. B. Parise and K. W. Chapman, *ACS Mater. Lett.*, 2021, **3**, 698–703.
29 C. Mottillo and T. Friščić, *Molecules*, 2017, **22**, 144.
30 CCDC 2421152: Experimental Crystal Structure Determination, 2026, DOI: 10.25505/fiz.icsd.cc2m8dp0.